ACS OMEGA

http://pubs.acs.org/journal/acsodf

Article

Design and Use of a Gold Nanoparticle−Carbon Dot Hybrid for a FLIM-Based IMPLICATION Nano Logic Gate

Shweta Pawar, Hamootal Duadi, Yafit Fleger, and Dror Fixler*

Cite This: *ACS Omega* 2022, 7, 22818−22824

Read Online

ACCESS | Metrics & More | Article Recommendations | Supporting Information

ABSTRACT: The interest in nanomaterials resides in the fact that they can be used to create smaller, faster, and more portable systems. Nanotechnology is already transforming health care. Nanoparticles are being used by scientists to target malignancies, improve drug delivery systems, and improve medical imaging. Integration of biomolecular logic gates with nanostructures has opened new paths in illness detection and therapy that need precise control of complicated components. Most studies have used fluorescence intensity techniques to implement the logic function. Its drawbacks, mainly when working with nanoparticles in intracellular media, include fluctuations in excitation power, fluorophore concentration dependence, and interference from cell autofluorescence. We suggest using fluorescence lifetime imaging microscopy (FLIM) in order to circumvent these constraints. Designing a nanohybrid composed of gold nanoparticles (AuNPs) and red-emitting carbon dots (CDs) can be used to develop a FLIM-based logic gate that can respond to multiple input parameters. Our findings indicate a nanohybrid that can serve as a nano-computer to receive and integrate chemical and biochemical stimuli and produce a definitive output measured by FLIM. This can open a new research avenue for enhanced diagnostics and therapy that require complicated factor handling and precise control. The AuNPs are conjugated to CDs' surfaces through a strong covalent linkage. The AuNP−CD nanohybrid shows fluorescence lifetime (FLT) quenching of pristine CDs after conjugation to AuNPs. The FLT was reduced from 3.61 ± 0.037 to 2.48 ± 0.040 ns. This quenched FLT can be recovered back by using trypsin as a recovering agent, giving us a reversible logic output. The FLT was recovered to 3.01 ± 0.01 ns after trypsin addition. This "on−off−on" response can be used to construct the IMPLICATION logic gate.

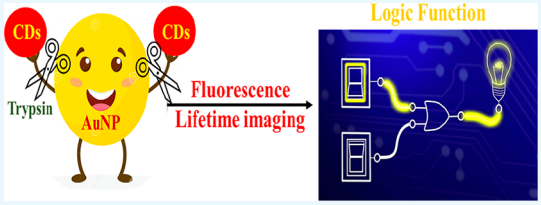

1. INTRODUCTION

Recent advances in nanotechnology have promoted the development of diverse biomedical applications.[1−3] Combining the logic gates with nanomaterials has paved innovative avenues in disease diagnostic and therapy (theranostics) that comprises precise control and handling of complex factors.[4,5] Nanomaterials of various types have unique physicochemical and surface properties that can improve activity and *in vivo* bioavailability of various therapies.[6] In particular, stimulus-responsive nanomaterials, which respond to environmental factors such as enzymes, pH, light, or temperature, can enhance therapy specificity and lower potential side effects.[7−10] However, the accuracy and precision of such nanomaterials remain limited by disease heterogeneity and the complex *in vivo* environment.[11] The recent combination of logic gates with nanoparticles has emerged as a potentially effective solution to address these challenges[4] and can open new paths in disease diagnostics and therapy (theranostics) that require precise control and handling of complex factors. Logic gates were originally defined as physical or computational devices implementing Boolean logic operations upon receiving inputs and generating specific outputs.[12] This computational concept of logic gates can be applied to the design of nanomaterials with intelligent stimulus-activation by single or multiple inputs—including chemical or biological inputs such as ion flux, catalysis, or affinity to relevant molecules.[12−14] Current stimulus-responsive nanomaterials are mostly considered as "YES/NO" gated devices.[15] Yet, these are inadequate for defining biological conditions, particularly in biosensing and disease diagnosis. Thus, efforts have been made to develop nanodevices incorporating logic gates that can execute complex information processes.[16]

Personalized logic function within living bodies can be achieved using gold nanoparticles (AuNPs) as they have tremendous biomedical and biochemical applications.[17−19] AuNPs are popular due to their non-toxic nature, easy modification,[20,21] biocompatibility,[22] and tunable optical properties[23] along with a wide absorption cross section.[24] To use AuNPs for fluorescence-based logic operation, they should be combined with a fluorophore. Carbon dots (CDs) are recently developed fluorescent carbon nanomaterials with excellent optical and structural properties, which can address a

Received: April 20, 2022
Accepted: June 8, 2022
Published: June 20, 2022

https://doi.org/10.1021/acsomega.2c02463
ACS Omega 2022, 7, 22818−22824

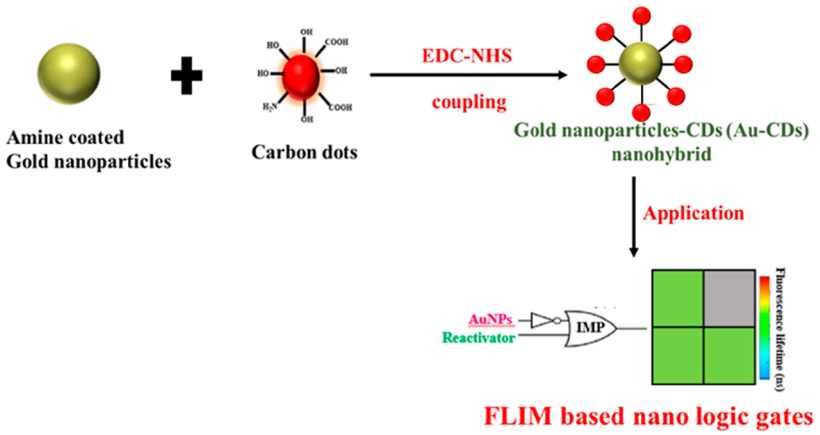

Figure 1. Schematic representation of FLIM nano logic gates based on AuNP−CD (gold nanoparticle−carbon dot) nanohybrid.

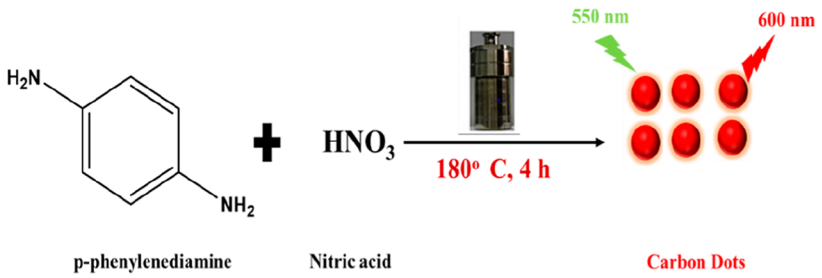

Figure 2. Schematic representation of the synthesis of red-emitting CDs. The CDs were synthesized *via* hydrothermal treatment of *p*-PD and nitric acid.

variety of logic functions.[13] The CDs are suitable candidates due to their chemical inertness, biocompatibility, facile functionalization, and high photostability.[25−27] CDs emitting in the near-infrared window are of significant importance for biological logic functions due to their high electromagnetic radiation penetration depth and minimum autofluorescence of tissue.[28−30] Nanohybrids formed between AuNPs and CDs have potential to serve as novel fluorescent nanomaterials, and as such these hybrids can retain the optical properties of both nanoparticles and CDs.

Fluorescence lifetime (FLT) imaging microscopy (FLIM) is a highly advanced functional microscopy technique, which can be used to implement fluorescent-based logic gates.[31,32] In contrast to conventional fluorescence intensity (FI) methods, FLIM is independent of both the power of the excitation source and dye concentration. FLT can be altered by reactions between AuNPs and CDs, and variations in the proximity between AuNPs and CDs can be deduced more accurately by FLT than by FI. Due to these features, development of an AuNP−CD (AuCD) nanohybrid has potential to serve as a useful FLIM nanoprobe.[33] The challenge is combining AuNPs and CDs to generate a new nanohybrid[34] containing FLIM-based logic gates that can serve for various biomedical applications.

In this study, we describe nanohybrids made up of biocompatible fluorophores like CDs and AuNPs that can be utilized to make FLIM-based nano logic gates. CDs were incorporated on the surface of AuNPs by 1-ethyl-3-(3-dimethyl-aminopropyl)carbodiimide hydrochloride (EDC)−*N*-hydroxy succinimide (NHS) coupling to create the nanosized fluorescent hybrid (Figure 1). To obtain the appropriate fluorescence logic output, we will use AuNPs and trypsin as inputs. As a result, CDs can be used as a nanoscale IMPLICATION (IMP) logic gate, with AuNPs and trypsin as chemical inputs and the FLIM data as the output. Designing a reversible logic output with CDs, quenching its fluorescence with AuNPs, and recovering with trypsin are part of our technique. Because of its reversible system, the synthesized nanohybrid can be used to make reusable NP devices.

2. MATERIALS AND METHODS

2.1. Preparation of Samples. *2.1.1. Preparation of Red-Emitting CDs.* The red-emitting CDs were synthesized through hydrothermal treatment on *p*-phenylenediamine (*p*-PD) and nitric acid with the concentration ratio of c[*p*-PD]/c[HNO_3] to be 2.5. Here, the *p*-PD acts as a carbon source, while nitric acid is used for nitrogen doping. The mixture was thermalized at 180 °C for 4 h in an autoclave inside the furnace (Figure 2). After that, the obtained solution was subjected to centrifugation at 20 000 rpm for 30 min and the supernatant was collected and lyophilized.

2.1.2. Purification of Red-Emitting CDs. The obtained CDs, prepared with the aid of volatile acid (HNO_3), were separated to the acid-contained crude products by solvent evaporation. Crude products were washed repeatedly with hexane to remove the unreacted *p*-PD and then centrifuged at 14 000 rpm for 30 min to remove any polymer precipitation. Finally, the solution was filtered through a 0.22 μm filter membrane to remove the precipitation. Purified CD solutions were dried to obtain CD powder by oven drying.

2.1.3. Preparation of PEG-Coated Gold Colloids. AuNPs were prepared *in situ* by addition of $HAuCl_4{\cdot}3H_2O$ to the PEG−NH_2 solution containing NaOH. In a typical process, 340 μL PEG and 0.75 mL of 1% NaOH were mixed in a 50 mL beaker with a magnetic stirrer and heated to 50 °C. Then,

https://doi.org/10.1021/acsomega.2c02463
ACS Omega 2022, 7, 22818−22824

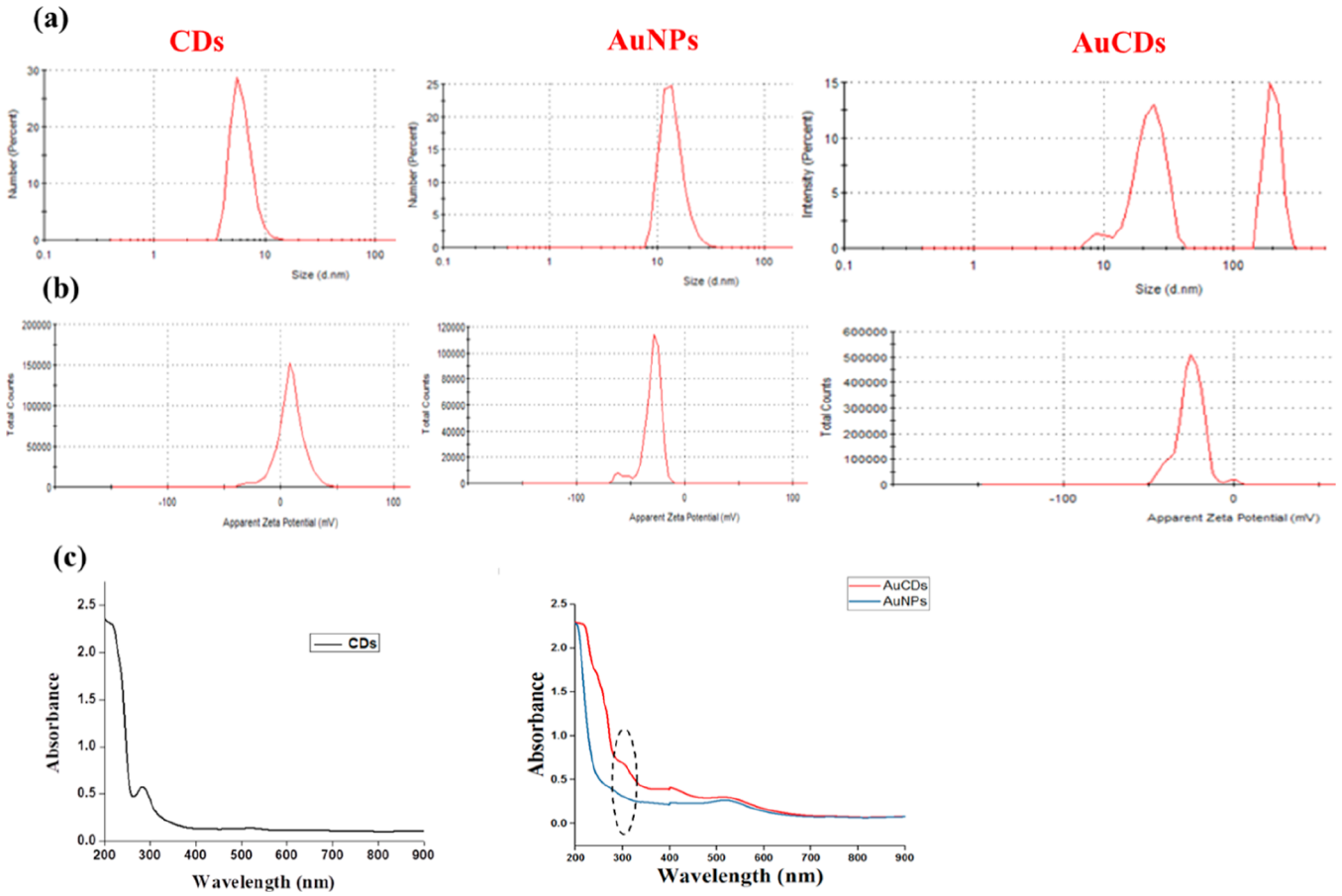

Figure 3. CDs, AuNPs, and AuCDs before and after conjugation: (a) DLS, (b) ζ potential measurements, and (c) absorption spectra.

19.74 mg of gold precursor ($HAuCl_4{\cdot}3H_2O$) was added under vigorous stirring. The resulting solution was slowly heated to 80 °C and stirred till the solution turned ruby red. The color change from transparent to ruby red confirmed the formation of PEG-coated AuNPs.

2.1.4. Preparation of AuCD Nanohybrid. The AuCD nanohybrid was created through an amide linkage between the CDs' carboxylic group and the AuNPs' surface amide groups. One mL of gold colloid and EDC solution (8 μL of 10 mg/mL) along with NHS (16 μL) were taken. The solution was vortexed and incubated for 30 min. The solution was then centrifuged at 3600 relative centrifugal field (rcf) for 5 min. 1 mL of PEG-coated AuNPs was mixed with 1 mg of purified CDs and then vortexed and mixed thoroughly and incubated overnight.

2.1.5. Materials. The gold salt ($HAuCl_4{\cdot}3H_2O$) was procured from the J and K Chemicals. Co. (Beijing China), while NaOH and *p*-PD were purchased from Sigma-Aldrich. Amine-terminated polyethylene glycol (NH_2−PEG−COOH) was purchased from Peng Shuo Biological Technology Co., Ltd. (Shanghai, China). EDC and NHS were purchased from Aladdin (Shanghai, China). The hexane used in the study was of analytical grade and was obtained from Sigma. Trypsin solution was acquired from Biological Industries. Analytical grade HNO_3 (70%) was procured from DAEJUNG Korea. All chemicals were of analytical grade and used without any further purification. Distilled water was used for the preparation of all the solutions.

2.1.6. FLIM Measurement. The AuCD sample was subjected to FLIM measurement in order to observe the changes in FLT before and after the conjugation and also after adding reagents. An inverted two-channel laser scanning confocal microscope system (DCS 120, Becker & Hickl GmbH, Berlin, Germany) was used to perform the FLT measurements presented in this paper. A 495 nm LP filter and a 1.0 mm pinhole were used to identify 256 × 256 pixel sample regions excited by 473 nm laser pulses. The software SPCImage v. 5.3 was used to create FLIM images (Becker & Hickl GmbH 2015, Berlin, Germany). FLT measurements were performed using scanning confocal PicoQuant micro time microscope (MT200) with time-correlated single-photon counting abilities.

2.1.7. Sample Characterization. Transmission electron microscopy (TEM) images were obtained using a JEOL JEM-1400 analytical TEM with an accelerating voltage of 120 kV. The ultraviolet (UV−vis) absorption spectra were recorded using a Shimadzu UV-1900 spectrophotometer. A Cary Eclipse spectrofluorometer (Varian, Palo Alto, CA, USA) was used to record the fluorescence spectra and relative quantum yield (QY) values. Rhodamine B (RhB) was used as a reference to measure the QY values of CDs.

3. RESULTS AND DISCUSSION

3.1. CDs, AuNPs, and AuCD Nanohybrid Characterization. The sizes of CDs, AuNPs, and AuCDs were measured by dynamic light scattering (DLS), and the sizes were found to be 6 ± 1.36 nm for CDs, 14 ± 3.68 nm for AuNPs, and two

https://doi.org/10.1021/acsomega.2c02463
ACS Omega 2022, 7, 22818−22824

peaks for AuCD nanohybrid at 23 ± 5.58 and 200 ± 26.74 nm (Figure 3a). The larger AuCD hybrid aggregates were generated when smaller AuCD nanohybrids were combined into larger particles.

The aggregates are of nanohybrid nature and this is confirmed through TEM images (Figure S6) and absorption data. There is no significant change in the plasmonic peak of AuNPs after the addition of CDs confirming non-aggregation of AuNPs in the solution (Figure 3c). The increase in size for AuCDs compared to AuNPs suggested the coupling of AuNPs on the surface of the CDs. The ζ potential for CDs, AuNPs, and AuCDs are 8.42 ± 11.80, −28.6 ± 6.17, and −25.8 ± 7.28 mV, respectively (Figures 3b and S1). These ζ values suggest that there is an electrostatic attraction between AuNPs and CDs for the hybrid formation, while the negative potential value of the nanohybrid formed confirms its stabilization. The UV absorption spectrum for CDs shows a peak at 284 nm, which is due to $\pi-\pi^*$ transitions of C−C structure.[35] The plasmonic peak for AuNPs was around 520 nm. However, the absorption spectra of AuCD nanohybrid were a combination of both AuNPs and CDs with UV−vis spectra (Figure 3c) further confirming the conjugation.

The synthesized CDs showed the typical behavior of excitation wavelength-dependent FI (Figure 4). We saw that

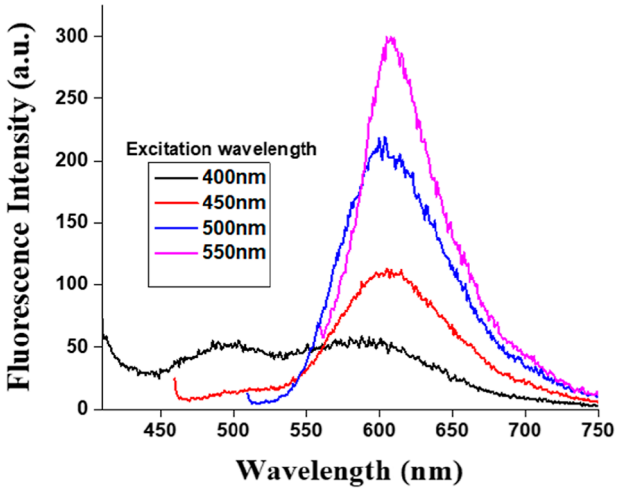

Figure 4. FI of red-emitting CDs when excited at different wavelengths. The graph demonstrates the excitation-dependent emission of CDs.

with increasing excitation wavelength, the emission bands were shifted bathochromically, which revealed the distribution of surface energy states on the CDs.[36] The QY values of the obtained CDs were found to be 3% (calculation given in the Supporting Information Section S1).

The TEM images presented in Figure 5 exhibit that the sample was well dispersed and the average sizes of the CDs, AuNPs, and AuCDs were 7.70 ± 0.56, 10 ± 4.51, and 57 ± 3.42 nm, respectively (Figures S2−S4).

The average particle sizes were analyzed using ImageJ software. The spherical morphology was also confirmed through this TEM analysis. Along with single nanohybrid, bigger aggregates are also observed (Figure S5). The CDs' FI remained nearly constant at different temperatures (Figure S6) ranging from 10 to 100 °C, indicating that they were stable at higher temperatures. The effect of pH on the CDs' FI was measured, as shown in Figure S6. The intensity of the

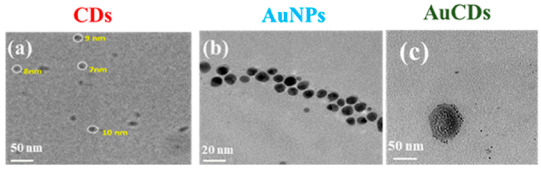

Figure 5. TEM images of (a) CDs, (b) AuNPs, and (c) AuCDs.

fluorescence increased as the pH values increased from 2 to 6 in the acidic zone but decreased between 8.0 and 14.0 in the alkaline region. Protonation of the amino groups on the surface of carbon dots generated the decreased FI in acidic conditions.

3.2. Steady-State and FLT Analysis. Next, we measured the FI and FLT of CDs and AuCD nanohybrids. We found a decrease in FI after addition of AuNPs to CDs (Figure 6a). Similarly, we also observed a decrease in FLT (Figure 6b) after CD−AuNP interaction; the average FLT of CDs significantly decreased from 3.61 ± 0.037 to 2.48 ± 0.040 ns (Table 1). These results indicate successful formation of the AuCD nanohybrid. The fluorescence quenching observed in FI steady-state measurements and shortening of the FLT are likely due to the change in the microenvironment before and after interaction of CDs and AuNPs, which resulted in different FLIM images for CDs and AuCDs (as seen in Figure 9).

3.3. Mechanism of Fluorescence Recovery. We next examined the mechanism of fluorescence quenching and recovery of the AuCDs. As shown above, the conjugation of CDs to AuNP led to quenching of the CD's fluorescence. This quenching may be either static, dynamic, or intramolecular. Assessment of CD lifetime values revealed a shortening of lifetime after CD conjugation to AuNPs (Figure S7); this change in lifetime rules out the possibility of static quenching of fluorescence. The strong covalent bond (amide linkage) that is formed between CDs and AuNPs indicates intramolecular quenching of CD fluorescence. The shortening of FLT is likely caused by the "through-bond" interaction[37] that occurs during formation of the nanohybrid (Figure 7).

Trypsin is a known peptide-cleaving enzyme; therefore, it could potentially break the amide bond that forms the AuCD nanohybrids. Thus, we tested the response of AuCD nanohybrids to treatment with trypsin, that is, whether trypsin can induce cleavage that would return CDs back to their original fluorescent state. To this end, trypsin was incubated with AuCDs (37 °C) and FLIM was then used to image lifetimes. Ground-state interactions between CDs, AuCDs, and trypsin are shown in Figure S8. FLIM images showed fluorescence of CDs alone, and then, fluorescence quenching after CD conjugation to AuNPs that created AuCDs (Figure 8). Notably, FLIM images taken after incubation of trypsin with AuCDs showed recovery of the fluorescent state. The FTIR spectrum of CDs showed a strong peak at 1515 cm^{-1}, indicating the presence of the −NH group, whereas the broad peak around 1345 cm^{-1} corresponded to −OH deformation vibrations. The covalent attachment of AuNPs onto the CD surface was confirmed by the shift of the carbonyl peak of carboxylic acid from 1623 to 1609 cm^{-1}, endorsing the formation of an amide linkage. After trypsin treatment, the peak again goes back to 1621 cm^{-1}, confirming the cleavage of the amide bond between CDs and AuNPs (Figure S9).

Figure 9 summarizes the mechanism of CD fluorescence quenching and recovery by AuNPs and trypsin.

https://doi.org/10.1021/acsomega.2c02463
ACS Omega 2022, 7, 22818−22824

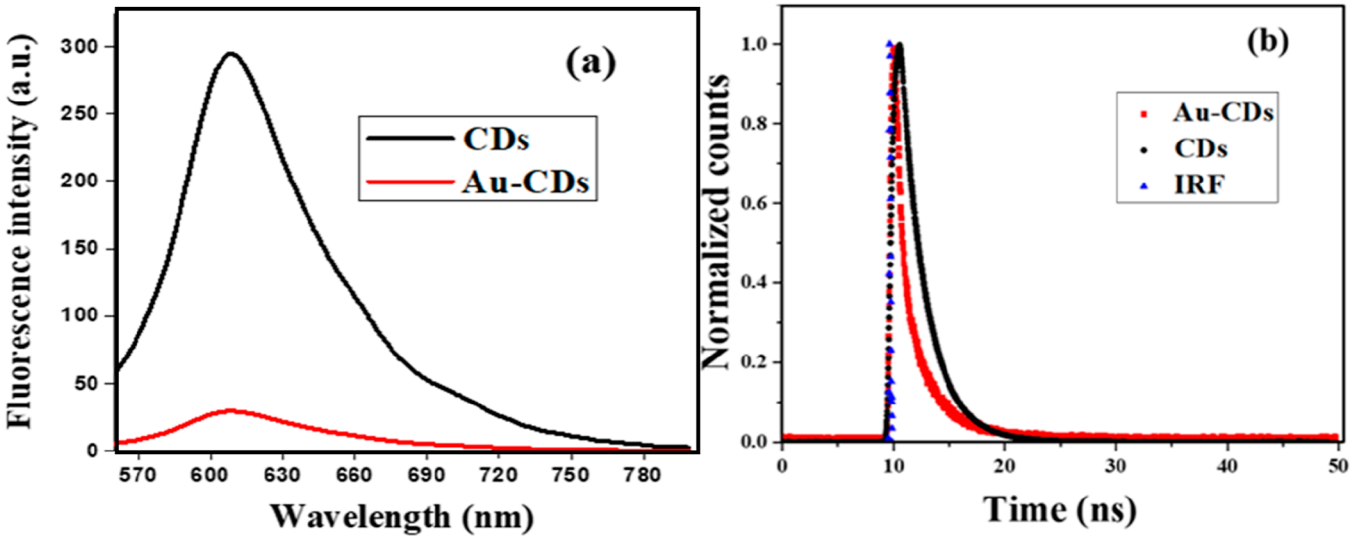

Figure 6. (a) FI and (b) time-resolved fluorescence decay curves of CDs and AuCDs in water. The blue points represent instrument response function.

Table 1. FLT of CDs and AuCDs Calculated from Time-Resolved Fluorescence Decay Curves

sample	α (%)	τ (ns)	χ^2
CDs	100	3.61 ± 0.037	1.01
AuCDs	100	2.48 ± 0.040	1.09

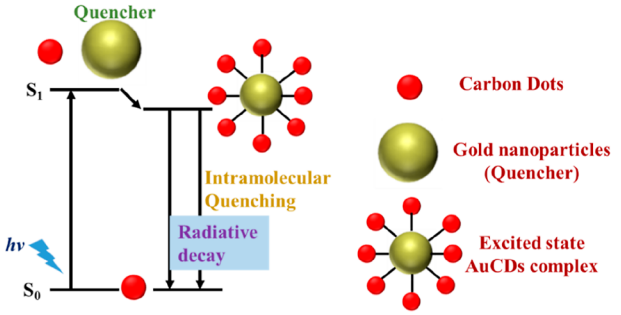

Figure 7. Schematic representation of the fluorescence quenching mechanism of AuCDs. Intramolecular quenching occurs when CDs interact covalently with AuNPs.

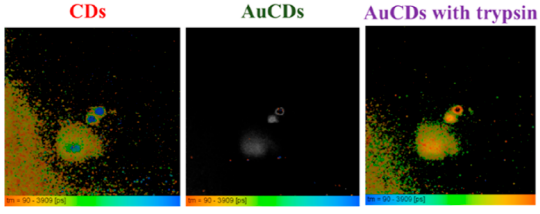

Figure 8. FLIM images of CDs, AuCDs, and of AuCDs with trypsin. Trypsin treatment returned CDs back to their original fluorescent state. Images were taken using a 473 nm laser.

3.4. Logic Gate Application. The AuCD nanohybrid can be used for logic operations based on FLT of CDs. We have defined "inputs" for our system as the presence of AuNPs or trypsin. Different logics possible in the system can be recognized by conditions such as no AuNPs and no trypsin (0, 0), presence of AuNPs and no trypsin (1, 0), absence of AuNPs and presence of trypsin (0, 1), and presence of both AuNPs and trypsin (1, 1). Chemical inputs such as the presence of either AuNPs or trypsin are represented by the Boolean "0" and "1" values. "0" indicates the absence of the AuNPs or trypsin (OFF state), while "1" indicates the presence of the AuNPs or trypsin (ON state) Figure 10.

The fluorescence variations of CDs were monitored (excitation: 473 nm) with two chemical inputs such as AuNPs and trypsin, the truth table (Table S1 and Figure S10) for the IMPLICATION function was obtained, while the ground-state interactions are shown with the absorption spectra Figure S8. To assign the logic function, we need to simply choose the current cut-off value for the system as defined as "output". The cut-off value was 2.48 ± 0.04 ns; above this lifetime value it was assigned ON, and below this the output is OFF. With AuNPs and trypsin as chemical inputs and FLIM image as the desired output, this unique optical response has been successfully leveraged to construct an IMPLICATION logic gate. The behavior of AuCD nanohybrid displays the FLIM-based nano logic gate ability. It is important to have a reversible logic system as irreversible schemes do not allow complex logic operations.[38] For an irreversible construct, it is impossible to recognize if there is a change in condition. In the case of the reversible system, these kinds of changes can be studied again without the insertion of a brand new construct into the system. It can reveal the condition repeatedly in either positive or negative direction.

The scheme of the FLIM-based nano logic gate is depicted in Figure 11.

4. CONCLUSIONS

In the present study, we developed a nanohybrid that incorporates CDs and AuNPs, and which can be efficient for constructing FLIM-based logic gates. Logic operations were defined by chemical and biochemical inputs and by FLIM imaging output of the nanohybrid.

FLIM is a valuable tool for logic gate definitions due to the ability to select precise cut-off values. Although FI-based logic gates cannot be predefined, as they depend upon both the detection and excitation parameters, FLT values do not depend on these parameters, or on nanoparticle concentration, and are much more reproducible and quantifiable.

https://doi.org/10.1021/acsomega.2c02463
ACS Omega 2022, 7, 22818−22824

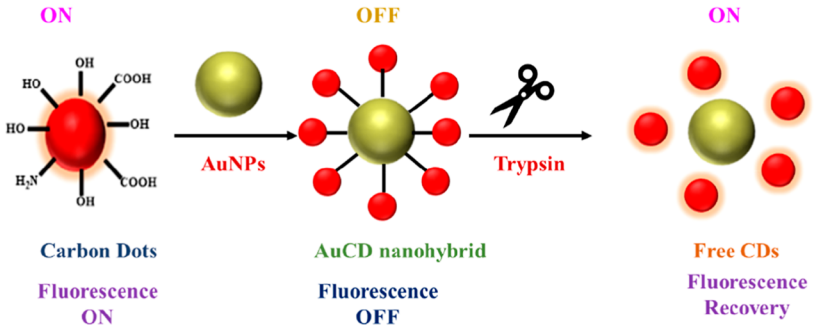

Figure 9. Scheme of the mechanism of fluorescence quenching and recovery. CD fluorescence is quenched after conjugation to AuNP and recovered *via* trypsin cleavage of the amide bond between the AuNPs and CDs.

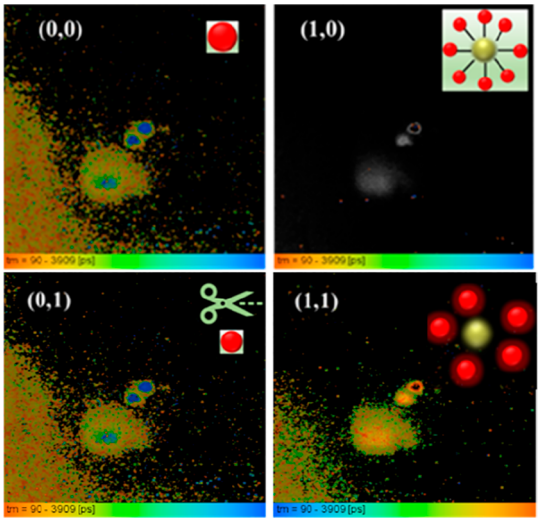

Figure 10. FLIM images of CDs in the presence of AuNPs and trypsin as chemical inputs, and FLIM image as the output.

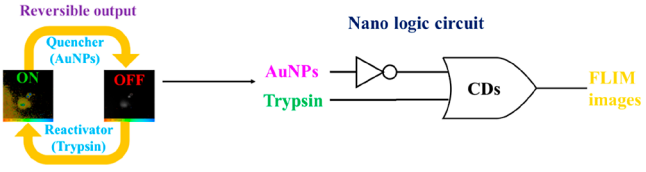

Figure 11. Scheme of the AuCD nanohybrid displaying a FLIM logic gate behavior and its reversibility.

Here, we used red-emitting CDs, with emission profiles in the infrared region. This feature can enable future use of AuCDs *in vivo* due to high penetration of infrared light through tissues. In addition, the AuCDs comprise a reversible system that can enable future construction of reusable nanodevices. Future studies can also modify the nanohybrid to affect behavior of the next construct in the logic network and thus provide functions similar to computer-like logic.

■ ASSOCIATED CONTENT

Supporting Information

The Supporting Information is available free of charge at https://pubs.acs.org/doi/10.1021/acsomega.2c02463.

QY measurements, fit curve of ζ potential of CDs, AuNPs, and AuCD nanohybrid, histograms and Gaussian fittings of particle size distribution of the CDs, histograms and Gaussian fittings of particle size distribution of the AuNPs, histograms and Gaussian fittings of particle size distribution of the AuCDs, TEM images of bigger size aggregates of AuCDs, effect of temperature and pH on the carbon dots, (a) FI and (b) time-resolved fluorescence decay curves of AuCDs after addition of trypsin (λ_{ex} = 473 nm), normalized absorption spectra of CDs, CDs + trypsin, AUCDs, and AUCDs + trypsin, FTIR spectra of CDs, AuCDs, and AuCDs after trypsin treatment to elucidate the mechanism, fluorescent response of CDs in the presence of AuNPs and trypsin as chemical inputs, to function in an IMPLICATION logic gate, and truth table for IMPLICATION logic gate (PDF)

■ AUTHOR INFORMATION

Corresponding Author

Dror Fixler − *Faculty of Engineering, Bar Ilan University, Ramat Gan 5290002, Israel; Bar-Ilan Institute of Nanotechnology & Advanced Materials (BINA), Bar Ilan University, Ramat Gan 5290002, Israel;* orcid.org/0000-0003-0963-7908; Email: Dror.Fixler@biu.ac.il

Authors

Shweta Pawar − *Faculty of Engineering, Bar Ilan University, Ramat Gan 5290002, Israel; Bar-Ilan Institute of Nanotechnology & Advanced Materials (BINA), Bar Ilan University, Ramat Gan 5290002, Israel*

Hamootal Duadi − *Faculty of Engineering, Bar Ilan University, Ramat Gan 5290002, Israel; Bar-Ilan Institute of Nanotechnology & Advanced Materials (BINA), Bar Ilan University, Ramat Gan 5290002, Israel*

Yafit Fleger − *Bar-Ilan Institute of Nanotechnology & Advanced Materials (BINA), Bar Ilan University, Ramat Gan 5290002, Israel*

Complete contact information is available at: https://pubs.acs.org/10.1021/acsomega.2c02463

Notes

The authors declare no competing financial interest.

■ ACKNOWLEDGMENTS

S.P. thanks the Planning and Budgeting Committee (PBC) of the Council for Higher Education of Israel and Ministry of Science Technology and Space, Israel−Russia 205553, for supporting with a fellowship.

https://doi.org/10.1021/acsomega.2c02463
ACS Omega 2022, 7, 22818−22824

REFERENCES

(1) Karimi, M.; Ghasemi, A.; Zangabad, P. S.; Rahighi, R.; Basri, S. M. M.; Mirshekari, H.; Amiri, M.; Pishabad, Z. S.; Aslani, A.; Bozorgomid, M.; Ghosh, D.; Beyzavi, A.; Vaseghi, A.; Aref, A. R.; Haghani, L.; Bahrami, S.; Hamblin, M. R. Smart Micro/Nanoparticles in Stimulus-Responsive Drug/Gene Delivery Systems. *Chem. Soc. Rev.* **2016**, *45*, 1457−1501.

(2) Fu, X.; Hosta-Rigau, L.; Chandrawati, R.; Cui, J. Multi-Stimuli-Responsive Polymer Particles, Films, and Hydrogels for Drug Delivery. *Chem* **2018**, *4*, 2084−2107.

(3) Dudchenko, N.; Pawar, S.; Perelshtein, I.; Fixler, D. Magnetite Nanoparticles: Synthesis and Applications in Optics and Nanophotonics. *Materials* **2022**, *15*, 2601.

(4) Barnoy, E. A.; Popovtzer, R.; Fixler, D. Fluorescence for Biological Logic Gates. *J. Biophotonics* **2020**, *13*, No. e202000158.

(5) Barnoy, E. A.; Fixler, D.; Popovtzer, R.; Nayhoz, T.; Ray, K. An Ultra-Sensitive Dual-Mode Imaging System Using Metal-Enhanced Fluorescence in Solid Phantoms. *Nano Res.* **2015**, *8*, 3912−3921.

(6) Mura, S.; Nicolas, J.; Couvreur, P. Stimuli-Responsive Nanocarriers for Drug Delivery. *Nat. Mater.* **2013**, *12*, 991−1003.

(7) Mal, N. K.; Fujiwara, M.; Tanaka, Y. Photocontrolled Reversible Release of Guest Molecules from Coumarin-Modified Mesoporous Silica. *Nature* **2003**, *421*, 350−353.

(8) Singh, N.; Karambelkar, A.; Gu, L.; Lin, K.; Miller, J. S.; Chen, C. S.; Sailor, M. J.; Bhatia, S. N. Bioresponsive Mesoporous Silica Nanoparticles for Triggered Drug Release. *J. Am. Chem. Soc.* **2011**, *133*, 19582−19585.

(9) Wang, W.; Cheng, D.; Gong, F.; Miao, X.; Shuai, X. Design of Multifunctional Micelle for Tumor-Targeted Intracellular Drug Release and Fluorescent Imaging. *Adv. Mater.* **2012**, *24*, 115−120.

(10) Tregubov, A. A.; Nikitin, P. I.; Nikitin, M. P. Advanced Smart Nanomaterials with Integrated Logic-Gating and Biocomputing: Dawn of Theranostic Nanorobots. *Chem. Rev.* **2018**, *118*, 10294−10348.

(11) Luo, C.; He, L.; Chen, F.; Fu, T.; Zhang, P.; Xiao, Z.; Liu, Y.; Tan, W. Stimulus-Responsive Nanomaterials Containing Logic Gates for Biomedical Applications. *Cell Rep. Phys. Sci.* **2021**, *2*, 100350.

(12) Ma, D.-L.; He, H.-Z.; Chan, D. S.-H.; Leung, C.-H. Simple DNA-Based Logic Gates Responding to Biomolecules and Metal Ions. *Chem. Sci.* **2013**, *4*, 3366−3380.

(13) Pawar, S.; Duadi, H.; Fleger, Y.; Fixler, D. Carbon Dots-Based Logic Gates. *Nanomaterials* **2021**, *11*, 232.

(14) Barnoy, E. A.; Motiei, M.; Tzror, C.; Rahimipour, S.; Popovtzer, R.; Fixler, D. Biological Logic Gate Using Gold Nanoparticles and Fluorescence Lifetime Imaging Microscopy. *ACS Appl. Nano Mater.* **2019**, *2*, 6527−6536.

(15) Lai, Y.-H.; Sun, S.-C.; Chuang, M.-C. Biosensors with Built-In Biomolecular Logic Gates for Practical Applications. *Biosensors* **2014**, *4*, 273.

(16) Macia, J.; Manzoni, R.; Conde, N.; Urrios, A.; de Nadal, E.; Solé, R.; Posas, F. Implementation of Complex Biological Logic Circuits Using Spatially Distributed Multicellular Consortia. *PLoS Comput. Biol.* **2016**, *12*, No. e1004685.

(17) Bansal, S. A.; Kumar, V.; Karimi, J.; Singh, A. P.; Kumar, S. Role of Gold Nanoparticles in Advanced Biomedical Applications. *Nanoscale Adv.* **2020**, *2*, 3764−3787.

(18) Hou, K.; Fixler, D.; Han, B.; Shi, L.; Feder, I.; Duadi, H.; Wang, X.; Tang, Z. Towards In Vivo Tumor Detection Using Polarization and Wavelength Characteristics of Self-Assembled Gold Nanorods. *ChemNanoMat* **2017**, *3*, 736−739.

(19) Hou, K.; Zhao, J.; Wang, H.; Li, B.; Li, K.; Shi, X.; Wan, K.; Ai, J.; Lv, J.; Wang, D.; Huang, Q.; Wang, H.; Cao, Q.; Liu, S.; Tang, Z. Chiral Gold Nanoparticles Enantioselectively Rescue Memory Deficits in a Mouse Model of Alzheimer's Disease. *Nat. Commun.* **2020**, *11*, 1−11.

(20) Haimov, E.; Weitman, H.; Polani, S.; Schori, H.; Zitoun, D.; Shefi, O. Meso-Tetrahydroxyphenylchlorin-Conjugated Gold Nanoparticles as a Tool To Improve Photodynamic Therapy. *ACS Appl. Mater. Interfaces* **2018**, *10*, 2319−2327.

(21) Blanco, E.; Shen, H.; Ferrari, M. Principles of Nanoparticle Design for Overcoming Biological Barriers to Drug Delivery. *Nat. Biotechnol.* **2015**, *33*, 941−951.

(22) Chakraborty, R.; Leshem-Lev, D.; Kornowski, R.; Fixler, D. The Scattering of Gold Nanorods Combined with Differential Uptake, Paving a New Detection Method for Macrophage Subtypes Using Flow Cytometery. *Nano Lett.* **2020**, *20*, 8360−8368.

(23) Jain, P. K.; Lee, K. S.; El-Sayed, I. H.; El-Sayed, M. A. Calculated Absorption and Scattering Properties of Gold Nanoparticles of Different Size, Shape, and Composition: Applications in Biological Imaging and Biomedicine. *J. Phys. Chem. B* **2006**, *110*, 7238−7248.

(24) El-Sayed, M. A. Some Interesting Properties of Metals Confined in Time and Nanometer Space of Different Shapes. *Acc. Chem. Res.* **2001**, *34*, 257−264.

(25) Wang, X.; Feng, Y.; Dong, P.; Huang, J. A Mini Review on Carbon Quantum Dots: Preparation, Properties, and Electrocatalytic Application. *Front. Chem.* **2019**, *7*, 671.

(26) Semeniuk, M.; Yi, Z.; Poursorkhabi, V.; Tjong, J.; Jaffer, S.; Lu, Z.-H.; Sain, M. Future Perspectives and Review on Organic Carbon Dots in Electronic Applications. *ACS Nano* **2019**, *13*, 6224−6255.

(27) Liu, M. L.; Chen, B. B.; Li, C. M.; Huang, C. Z. Carbon Dots: Synthesis, Formation Mechanism, Fluorescence Origin and Sensing Applications. *Green Chem.* **2019**, *21*, 449−471.

(28) Wei, J.; Hao, D.; Wei, L.; Zhang, A.; Sun, C.; Wang, R. One-Step Preparation of Red-Emitting Carbon Dots for Visual and Quantitative Detection of Copper Ions. *Luminescence* **2021**, *36*, 472−480.

(29) Yuan, K.; Zhang, X.; Li, X.; Qin, R.; Cheng, Y.; Li, L.; Yang, X.; Yu, X.; Lu, Z.; Liu, H. Great Enhancement of Red Emitting Carbon Dots with B/Al/Ga Doping for Dual Mode Anti-Counterfeiting. *Chem. Eng. J.* **2020**, *397*, 125487.

(30) Pan, L.; Sun, S.; Zhang, L.; Jiang, K.; Lin, H. Near-Infrared Emissive Carbon Dots for Two-Photon Fluorescence Bioimaging. *Nanoscale* **2016**, *8*, 17350−17356.

(31) Barnoy, E. A.; Motiei, M.; Tzror, C.; Rahimipour, S.; Popovtzer, R.; Fixler, D. Biological Logic Gate Using Gold Nanoparticles and Fluorescence Lifetime Imaging Microscopy. *ACS Appl. Nano Mater.* **2019**, *2*, 6527−6536.

(32) Datta, R.; Heaster, T. M.; Sharick, J. T.; Gillette, A. A.; Skala, M. C. Fluorescence Lifetime Imaging Microscopy: Fundamentals and Advances in Instrumentation, Analysis, and Applications. *J. Biomed. Opt.* **2020**, *25*, 071203.

(33) Chen, L.-C.; Lloyd, W. R.; Chang, C.-W.; Sud, D.; Mycek, M.-A. Fluorescence Lifetime Imaging Microscopy for Quantitative Biological Imaging. In *Methods in Cell Biology*; Academic Press, 2013; Vol. *114*, pp 457−488.

(34) Yan, Y.; Yu, H.; Zhang, K.; Sun, M.; Zhang, Y.; Wang, X.; Wang, S. Dual-Emissive Nanohybrid of Carbon Dots and Gold Nanoclusters for Sensitive Determination of Mercuric Ions. *Nano Res.* **2016**, *9*, 2088−2096.

(35) Pawar, S.; Togiti, U. K.; Bhattacharya, A.; Nag, A. Functionalized Chitosan−Carbon Dots: A Fluorescent Probe for Detecting Trace Amount of Water in Organic Solvents. *ACS Omega* **2019**, *4*, 11301−11311.

(36) Ding, H.; Li, X.-H.; Chen, X.-B.; Wei, J.-S.; Li, X.-B.; Xiong, H.-M. Surface States of Carbon Dots and Their Influences on Luminescence. *J. Appl. Phys.* **2020**, *127*, 231101.

(37) Green, S. A.; Simpson, D. J.; Zhou, G.; Ho, P. S.; Blough, N. V. Intramolecular Quenching of Excited Singlet States by StableNitroxyl Radicals. *J. Am. Chem. Soc.* **1990**, *112*, 7337−7346.

(38) Purkayastha, T.; Chattopadhyay, T.; De, D. Design of Reversible Logic Circuits Using Quantum Dot Cellular Automata-Based System. *Nanotechnol. Rev.* **2015**, *4*, 375−392.

https://doi.org/10.1021/acsomega.2c02463
ACS Omega 2022, 7, 22818−22824